Sperm-specific COX6B2 Enhances Oxidative Phosphorylation, Proliferation, and Survival in Lung Adenocarcinoma

Chun-Chun Cheng[1], Joshua Wooten[2], Kathleen McGlynn[1], Prashant Mishra[3], Angelique W. Whitehurst[1]*

[1]Department of Pharmacology, Simmons Comprehensive Cancer Center, UT Southwestern Medical Center, 5323 Harry Hines Blvd Dallas, Texas 75390-8807, USA.
[2]Nuventra, 3217 Appling Way, Durham, NC 27703
[3]Children's Research Institute, UT Southwestern Medical Center, Dallas, TX 75390, USA.

*Correspondence: Angelique.Whitehurst@UTSouthwestern.edu, 214-645-6066 (p), 214-645-6347 (f)

Running Title: COX6B2 promotes oxidative phosphorylation and survival in NSCLC.

Keywords: COX6B2, oxidative phosphorylation, cancer testis antigen, cytochrome c oxidase, hypoxia

Significance: COX6B2 a protein normally only expressed in testes is overexpressed in lung cancer and correlates with poor outcome in lung adenocarcinoma. Expression of COX6B2 enhances oxidative phosphorylation, proliferation, survival and growth of tumors in hypoxia.

Funding sources: AWW, CC, and KM were supported by NIH (R01CA196905). AWW and JW were supported by SU2C (SU2C-AACR-IRG1211). The UTSW shared tissue resource was supported by the Simmons Cancer Center Core grant from National Cancer Institute (P30CA142543).

The authors declare no potential conflicts of interest.

Abstract

Cancer Testes Antigens (CTAs) are genes whose expression is normally restricted to the testes but anomalously activated in cancer. A number of CTAs are implicated in supporting the unique energy-demands of sperm, however if and how these proteins contribute to metabolic pathways in tumors has not been investigated. Here we describe the mechanism of one such cryptic protein, COX6B2, a sperm-specific component of cytochrome c oxidase (CcO). COX6B2 is frequently expressed in human lung adenocarcinoma (LUAD), where it correlates with reduced patient survival. In tumor cells, COX6B2, but not its somatic isoform COX6B1, enhances activity of CcO, increasing ATP and NAD^+ generation. Consequently, COX6B2-expressing tumor cells display a proliferative advantage, particularly in low oxygen conditions. Conversely, depletion of COX6B2 attenuates ATP production, and causes a collapse in mitochondrial membrane potential leading to programmed cell death or senescence. Importantly, we find that COX6B2 is both necessary and sufficient for growth of tumors in vivo. Our findings reveal a previously unappreciated, tumor specific metabolic pathway that is hijacked from one of the most ATP-intensive processes in the animal kingdom: sperm motility.

Introduction

Tumors frequently activate genes whose expression is otherwise restricted to testes; these genes are known collectively as cancer-testes antigens (CT-antigens, CTAs). The expression of these genes outside their native and immune privileged site has been the basis for immunotherapeutic approaches including vaccines and adoptive T-cell therapy (1,2). Historically, functional knowledge of the contribution of these proteins, if any, to neoplastic behaviors has significantly lagged behind immune-targeting. In recent years, the functional characterization of CTAs has gained broader interest and these proteins have been implicated in tumor cell survival, TGF-β signaling, mitotic fidelity, polyadenylation, mRNA export, tumor suppressor silencing, and DNA damage repair (3-5). Together, an abundance of reports indicates that anomalous expression of testis proteins can be engaged to support the tumorigenic program. The biased expression pattern of these proteins to tumors and testes may offer an extraordinarily wide therapeutic window if they can be targeted directly.

One unique aspect of mammalian sperm physiology is the tremendous energy demand required for motility while preserving the integrity of their precious DNA cargo within the hostile environment of the female reproductive tract. To meet this demand, sperm contain a number of tissue specific protein isoforms for glycolysis and OXPHOS that mediate the increase in ATP production. For example, lactate dehydrogenase C, LDHC, is a testis-specific isoform of the terminal enzyme in glycolysis that catalyzes the reduction of pyruvate to lactate essential for male fertility (6-8). Similarly, COX6B2 is a testis-specific subunit of the cytochrome c oxidase (CcO, Complex IV). mRNA encoding of either LDHC or COX6B2 is undetectable in normal tissue, but both are upregulated in a number of different tumor derived cell lines (9),CTpedia (http://www.cta.lncc.br/index.php), classifying them as CTAs. However, it is unclear whether these proteins support metabolic programs in tumor cells.

In a large-scale loss of function analysis to annotate the contribution of individual CTAs to neoplastic behaviors, we found that COX6B2 is essential for survival of non-small cell lung cancer (NSCLC) cell lines (9). COX6B2 is a nuclear encoded, sperm-specific component of CcO (10). By transferring electrons from reduced cytochrome c to O_2, CcO is the rate-limiting step for ATP production by the electron transport chain (ETC). Thirteen subunits make up CcO: three are mitochondrial encoded and ten are derived from nuclear DNA. Six of the ten nuclear encoded subunits have tissue-specific isoforms that permit regulation of this complex in response to environmental cues (e.g. pH, hormones, metals, ATP/ADP ratio etc.) (11). The somatic isoform of COX6B2 is COX6B1, which is not expressed in sperm. These two proteins share 58% amino acid identity and ~80% similarity. Based on structural information, it is apparent that COX6B1/2 are the only CcO subunits that are not membrane bound. Instead, their localization is confined to the intermembrane space where cytochrome c associates. It is inferred that COX6B1/B2 participate in dimerization of CcO and cytochrome c association (12,13). While limited, studies on COX6B1 indicate that it is essential for CcO activity. In particular, human mutations in COX6B1 (R20C or R20H) abrogate CcO assembly and lead to severe cardiac defects (14). In addition, biochemical analysis indicates that removal of COX6B1 from assembled complexes enhances CcO activity, implying a negative regulatory role for COX6B1 (15). To-date no reports detail the function of COX6B2 nor indicate the physiological relevance of this sperm-specific subunit to fertility. Overall, compared to the enormous data on CcO in general, the COX6B proteins have been understudied.

We have undertaken a detailed investigation into the mechanism of action of COX6B2 when this protein is aberrantly expressed in NSCLC. Here, we report that COX6B2 enhances oxidative phosphorylation (OXPHOS) and ATP production in tumor cells. This activity accelerates proliferation in vitro and in vivo. In contrast, silencing of COX6B2 attenuates OXPHOS, reduces tumor cell viability and dramatically decreases growth in vivo. Importantly,

we find that hypoxia enhances COX6B2 expression, which confers a selective advantage for survival under low oxygen. Indeed, elevated COX6B2 mRNA correlates with reduced survival. Cumulatively, this study demonstrates the remarkable capacity of tumor cells to integrate primordial gene products into their regulatory environment as a means of promoting unrestrained proliferation. In turn, COX6B2 becomes a liability that may be exploited for tumor selective targeting of OXPHOS.

Materials and Methods

Cell lines

All NSCLC cell lines were obtained from John Minna (UT Southwestern) between 2014 and 2018. NSCLC cells were cultured in RPMI media supplemented with 5% FBS at 37°C, 5% CO_2 and 90% humidity. NSCLC cells were not passaged more than 10 times after thawing. Cells cultured under hypoxia followed the methods described previously (16), and each chamber attained oxygen concentration of ~2.5%. HEK293T cells were obtained from Gary Johnson (UNC) in 2010 and cultured in DMEM media supplemented with 10% FBS at 37°C, 5% CO_2 and 90% humidity. HEK293T cells were not passaged more than 3 times after thawing. All cells were authenticated between 2014 and 2020 using short tandem repeat profiling and periodically evaluated for mycoplasma contamination by DAPI stain for extra-nuclear DNA within one year of use.

Reagents

Chemicals and reagents were purchased from the following manufacturers: RPMI-1640 medium (R8758), DMEM (D6429), fetal bovine serum (FBS; F0926, batch# 17J121), HBSS (H8264), EGTA (E3889), fatty acid free BSA (A7030), oligomycin (O4876), CCCP (C2759), antimycin A (A8674), mannitol (M4125), KH_2PO_4 (P0662), $MgCl_2$ (M8266), ADP-K^+ salt (A5285), ascorbate (A5960), *N,N,N′,N′*-Tetramethyl-*p*-phenylenediamine dihydrochloride

(TMPD; 87890), sodium pyruvate solution (S8636), L-glutamine (G7513), dodecyltrimethylammonium bromide (DTBA; D8638), and DAPI (D9542) were purchased from MilliporeSigma. HEPES (BP410), sucrose (50-712-768), EDTA (S311), Tris Base (BP152), formaldehyde (BP521), and Hoechst 3342 (PI62249) were purchased from Fisher Scientific. Seahorse XF Plasma Membrane Permeabilize (XF PMP; 102504-100) are from Agilent.

Human LUAD tissues. All human LUAD tissues were obtained from the UTSW Tissue Resource in compliance with guidelines for informed consent approved by the UTSW Internal Review Board committee. Samples were homogenized in RIPA buffer (50 mM Tris-HCl pH7.4, 150 mM NaCl, 1% Triton X-100, 0.5% Sodium Deoxycholate, 0.1% SDS, 1 mM EDTA, 10 mM NaF, 1μg ml^{-1} pepstatin, 2μg ml^{-1} leupeptin, 2μg ml^{-1} aprotinin and 50μg ml^{-1} bestatin). The protein was recovered by centrifuge and quantitated by Pierce™ BCA Protein Assay Kit (23227, Thermo Fisher Scientific).

Kaplan-Meier analyses. Overall survival and time to first progression graphs were generated using kmplotter http://www.kmplot.com/lung) (17). In NSCLC, probability of overall survival (OS) was based on 1144 patients and time to first progression (FP) in 596 patients. In lung andenocarcinoma (LUAD), OS was based on 672 patients and FP on 443 patients. In lung squamous cancer (LUSC), OS was based on 271 patients and FP on 141 patients. Hazard ratios and p-values were calculated by Cox Regression Analysis.

Immunoblotting. SDS-PAGE and immunoblotting were performed as previously described (9). Antibodies used for immunoblotting were as follows: COX6B2 (1:1000, SAB1401983, MilliporeSigma), COX6B1 (1:1000, sc-393233, Santa Cruz Biotechnology), COX IV (1:5000, 4850, Cell Signaling Technology), β-Actin (1:10,000, sc-47778, Santa Cruz Biotechnology), V5 (1:5000, R960-25, Thermo Fisher Scientific), HIF-1α (1:1000, 610959, BD Biosciences), Cleaved Caspase-3 (1:500, 9661, Cell Signaling Technology), PARP (1:1000, 9532, Cell

Signaling Technology), ERK (1:3000, sc-135900, Santa Cruz Biotechnology), NDUFA9 (1:1000, 459100, Thermo Fisher Scientific).

Immunofluorescence. Cells plated on glass coverslips were washed with PBS, fixed with 4% formaldehyde for 15 minutes at room temperature (RT) and blocked for 3 hours at RT in blocking buffer (5% BSA in PBS with 0.1% Saponin). Cells were incubated with primary antibodies diluted with blocking buffer overnight at 4°C followed by washes and incubation with Alexa Fluor®-conjugated secondary antibodies (Thermo Fisher Scientific) for 1 hour at RT. ProLong™ Gold Antifade reagent with DAPI (Thermo Fisher Scientific) was used to mount slips on glass slides and images were acquired by Zeiss LSM510 confocal microscope. Antibodies used: COX6B2 (1:50, SAB1401983, MilliporeSigma), Tom20 (1:200, sc-17764, Santa Cruz Biotechnology).

Expression plasmids. Human COX6B2 and COX6B1 were obtained in pDONR223 (DNASU) and cloned into pLX302 and pLX304 respectively using the Gateway® Cloning system (Thermo Fisher Scientific). psPAX2 and pMD2.G lentiviral constructs were purchased from Addgene. For shRNA experiments, pLKO.1 vectors from TRC expressing COX6B2-targeted shRNAs (TRCN0000046119-122; sequences: 5'-CCGGGAGCAGATCAAGAACGGGATTCTCGAGAATCCCGTTCTTGATCTG CTCTTTTTG-3', 5'-CCGGGATCCGTAACTGCTACCAGAACTCGAGTTCTGGTAGCAGTTA CGGATCTTTTTG-3', 5'-CCGGCTACCAGAACTTCCTGGACTACTCGAGTAGTCCAGGAAG TTCTGGTAGTTTTTG-3', 5'-CCGGCCAGCCAGAACCAGATCCGTACTCGAGTACGGATCT GGTTCTGGCTGGTTTTTG-3') were used as shRNA pool. Nontargeting shRNA in pLKO.1 (shSCR) was used as a control (Addgene). For sgRNA experiments, pSpCas9(BB)-2A-GFP (PX458) was purchased from Addgene.

Lentiviral transduction Lentivirus was produced through co-transfection of HEK293T cells with 5 μg of viral expression vector, 3 μg of psPAX2 packing vector, and 2 μg of pMD2.G

envelope vector. Virus-conditioned medium was harvested, passed through 0.45-μm-pore-size filters, and then used to infect target cells in the presence of 10 μg/ml Sequa-brene™ (S2667, MilliporeSigma).

Mitochondrial content and mass analysis. Mitochondrial DNA quantification was performed as described (18). To detect mitochondrial mass, cells were incubated with 50 nM MitoTracker™ Green (Fisher Scientific) at 37°C for 25 minutes and processed according to manufacturer's protocol.

Metabolic assays. The oxygen consumption rate (OCR) and extracellular acidification rate (ECAR) were performed by using the Seahorse XFe96 Extracellular Flux analyzer (Agilent). Cells were plated in the XFe96 cell culture plates at a density of 10,000 cells (HCC515) or 5000 cells (H2122) in 80 μl of growth medium overnight to generate a confluent monolayer of cells. The assay medium consisted of 10mM glucose, 2mM glutamine, 1mM pyruvate in DMEM (D5030, MilliporeSigma). The reaction was monitored upon serial injections of oligomycin (5 μM), CCCP (1 μM), and antimycin A (2 μM). Results were normalized to total protein amount as determined by Pierce™ BCA Protein Assay Kit. Non-mitochondrial respiration is subtracted from the presented data. COX6B2 depleted cells were assessed following 8 days of shRNA or 3 days of siRNA. Respiratory activity of isolated CcO in permeabilized cells was performed as described (19,20) with modifications. Cells were permeabilized by XF PMP (1nM) and treated with CcO substrates (Ascorbate 10mM, TMPD 100μM).

Measurement of ATP. Cell-Titer Glo® (Promega) (CTG) was performed by manufacture's protocol with modification. 15 μl of CTG was used for 100 μl of cells in media. Data were normalized to total protein amount as determined by Pierce™ BCA Protein Assay Kit. Luminescence was read using a Pherastar® Plus plate reader (BMG Labtech).

NAD^+/NADH assay. Cells were plated into 96-well tissue culture plates (Corning), allowed to adhere overnight and reach 80-90% confluency. Cells were processed according to the

manufacturer's protocols for NAD^+/NADH-Glo Assay™ (Promega) with modification as previously described (21). NAD^+/NADH measured in COX6B2 depleted cells were transduced with shRNA for 8 days.

Blue native PAGE (BN-PAGE). Mitochondria isolation and BN-PAGE were performed as previously described with additional modifications (22-24) Specifically, mitochondrial fractions were collected in buffer containing 200 mM Sucrose, 10 mM Tris and 1mM EGTA/Tris. Mitochondria (50 μg) were solubilized in 20 μl buffer containing 50 mM NaCl, 50 mM Imidazole/HCl, 2 mM 6-Aminocaproic acid, 1mM EDTA, and digitonin (digitonin/protein ratio of 6g/g) for 30 minutes at 4°C. Solubilized proteins were supplemented with Coomassie brilliant blue G-250 digitonin/Coomassie dye in a ratio of 4:1, separated on NativePAGE™ Bis-Tris gels (3-12%, Thermo Fisher Scientific), and stained by Colloidal Blue (Thermo Fisher Scientific) or immunoblotted. NativeMark™ Unstained Protein Standard (Thermo Fisher Scientific) was used as a marker.

Measurement of Reactive Oxygen Species (ROS). The Fluorescent probe MitoSOX Red™(ThermoFisher) was used to measure superoxide. MitoSOX Red™ is a mitochondrial membrane dependent dye and therefore could not be used in COX6B2 depleted cells as they lose mitochondrial membrane potential ($\Delta\Psi_m$). In this case, Chloromethyldichlorodihydrofluorescein diacetate (CM-H2DCFDA, Fisher Scientific), detecting H_2O_2, was used for total ROS analysis in cells 11 days of shRNA silencing. For MitoSOX Red™ assay, 3 x 10^5 cells were stained by MitoSOX Red™ (5 μM; in HBSS) at 37°C for ten minutes. As a positive control, cells were treated with 50 μM antimycin A during staining. For CM-H2DCFDA assay, cells reaching approximately 80% confluency in 6-well dishes were stained by CM-H2DCFDA (5 μM; in HBSS) at 37°C for 20 minutes, washed with HBSS, and then recovered in culture media at 37°C for 15 minutes. Cells were immediately analyzed by flow cytometry using a BD LSRFortessa™ instrument and BD FACSDiva™ 6.2

software. A minimum of 20,000 cells were analyzed per condition. Data were analyzed by FlowJo® (v10). Forward scatter (FSC) and side scatter (SSC) parameters were used to exclude cellular debris, dead cells, and doublets to retain viable single cell events. The median fluorescent intensities in each group were used to calculate the fold change compared to the CTRL group.

EdU incorporation assays. Cells were exposed to ethynyl deoxyuridine (EdU) for 1 hour before fixing the cells in 4% formaldehyde. Cells were stained using the protocol for Click-iT™ EdU Alexa Fluor 488 Imaging Kit (Thermo Fisher) and co-stained with Hoechst 3342. Cells were quantified using fluorescence microscopy. EdU detected in COX6B2 depleted cells were transduced with shRNA for nine days.

Proliferation measurements. Cell proliferation was measured as described (21). HCC515 and H2122 cells were plated in replicates in 96-well plate with an initial seeding density of 1,200 cells and 700 cells respectively. The proliferation rate was calculated using the following formula: Proliferation Rate (Doublings per day) = Log_2 (Final cell count (day 5)/Initial cell count (day 1))/4 (days).

Soft-agar assays. Cells were seeded at a density of 50,000 cells (HCC515) or 5000 cells (H2122) per 12-well plate and treated as previously described (25). After three weeks, colonies were stained overnight with 0.01% crystal violet. Images were captured with a dissecting microscope, and quantitated by ImageJ software.

Gene expression. RNA was isolated using a mammalian total RNA isolation kit (RTN350, Sigma) and treated with DNase I (AMPD1, Sigma) according to the manufacturer's instructions. Equal microgram volumes of RNA were reverse transcribed for each experimental condition by the use of a High-Capacity cDNA reverse transfection kit (4368813, ThermoFisher Scientific) with oligo dT (12577-011, ThermFisher Scientific). The resulting cDNA was used for expression analysis performed with an Applied Biosystems real-time PCR system with TaqMan® real-time

PCR probes (Thermo Fisher). The TaqMan® qPCR probes were as follows: COX6B2 (Hs00376070_m1), COX6B1 (Hs01086739_g1). RPL27 (Hs03044961_g1) was used as an internal loading assay for all expression assays.

Transfections. siRNAs were reverse transfected with Lipofectamine® RNAiMAX (13778, Thermo Fisher Scientific) following the manufacturer's instructions. siRNAs against COX6B2 (sense sequence: COX6B2#1: 5'-GGAACGAGCAGATCAAGAA-3'; COX6B2#2: 5'-GCCAGAACCAGATCCGTA A-3') were purchased from Dharmacon and Sigma respectively. siGENOME Non-Targeting siRNA Pool #2 was used as a negative control (siCTRL). sgRNAs were forward transfected in 6-well dishes by using 6 μl of FuGENE® HD (PRE2311, Fisher Scientific) with 3 μg of sgRNA. Guide sequences of COX6B2 sgRNA are as following:

oligo #1: 5'-CACCGCGGCGTCGAC CATTTCCCCTTGG-3',

oligo #2: 5'-CACCGCGTCGACCATTTCCCCTTGGGG-3',

oligo #3: 5'-CACCGACATCCAACATCCACGAAGGAGG-3'.

Measurement of mitochondrial membrane potential. Following six days of shRNA (3×10^5 cells), cells were collected and resuspended in HBSS containing 0.2 μM JC-1 and incubated at 37°C in a CO_2 incubator for 25 minutes. The stained cells were collected by centrifuge and washed twice with HBSS containing 1% FBS. Then cells were resuspended in 500 μl of 1% FBS HBSS buffer. Cells were immediately analyzed by flow cytometry using a BD LSRFortessa™ instrument and BD FACSDiva™ 6.2 software. A minimum of 20,000 cells were analyzed per condition. FlowJo® (v10) was used to generate scatter plots.

Annexin-V staining. After 7 days of shRNA-mediated knockdown 1×10^5 cells were wash once in PBS and resuspend in Annexin-V Binding Buffer (422201, BioLegend) with 3 μl of Annexin-V-APC (640941, BioLegend) and DAPI (200 ng/ml), and incubated for 15 minutes at room temperature in the dark. Cells were immediately analyzed by flow cytometry using a BD LSRFortessa™ instrument and BD FACSDiva™ 6.2 software. A minimum of 20,000 cells were

analyzed per condition. FlowJo® (v10) was used to generate scatter plots. Early-stage apoptotic cells are presented in the lower right quadrants (Annexin-V positive and DAPI negative) and late-stage apoptotic cells are presented in the upper right quadrants (Annexin-V positive and DAPI positive).

Senescence associated β-galactosidase activity. Cells were stained by using Senescence Beta-Galactosidase Staining Kit following 11 days of shRNA (9860, Cell Signaling Technology) according to the manufacture's protocol. Cultures were examined under phase-contrast microscopy to determine the percentage of positive cells with blue precipitate.

Xenograft experiments. All animal experiments were conducted under a UT-Southwestern IACUC approved protocol. Hsd:Athymic Nude-Foxn1^{nu} female mice were purchased from Envigo. At six to eight-weeks of age (23-25 grams) mice were randomly assigned to the indicated groups. 2 x 10^6 cells in 100 µl PBS were subcutaneously injected in the flank. Once tumors were visible, tumor volume was measured by caliper in two dimensions, and volumes were estimated using the equation V = length x width^2/2. Caliper measurements were made twice a week.

Statistical analysis. Graphpad Prism (Graphpad Software) was used to perform all statistical analyses. Data were assessed for normality by Shapiro-Wilk tests. Unpaired Student's *t*-test was used for data with a normal distribution. Mann-Whitney test was used for data that did not conform to a normal distribution. *P* values less than or equal to 0.050 were considered significant.

Results

COX6B2 is expressed in LUAD tumors and correlates with poor survival

Using a large-scale functional genomics approaches, we previously found that depletion of COX6B2 activates cleaved caspase 3/7 in cell lines derived from breast, melanoma and

NSCLC, with the most potent activation in H1299 NSCLC cells (Supplementary Fig. S1A). Based on these findings, we examined the relationship between COX6B2 expression and patient outcome in NSCLC. Strikingly, elevated expression of COX6B2 is associated with significantly shorter overall survival (OS) time (P = 5.3 x10^{-6}, log rank test; HR: 1.46; 95% confidence interval (*CI*): 1.24-1.73 (**Fig. 1A**). In addition, COX6B2 expression positively correlates with time to first progression (FP) (P = 4.1 x10^{-4}, log rank test; HR: 1.63; 95% CI: 1.24-2.14 (**Fig. 1A**). Separation of the two major histological subtypes of NSCLC revealed a strong correlation for both outcomes in LUAD (OS: P = 1.6 x10^{-4}, log rank test; HR: 1.59; 95% CI: 1.25-2.03; FP: P = 9.4 x10^{-5}, log rank test; HR: 1.91; 95% CI: 1.37-2.65 (**Fig. 1B**). However, this correlation is not observed in lung squamous carcinoma (OS: P = 0.75, log rank test; HR: 1.05; 95% CI: 0.77-1.44; FP: P = 0.96, log rank test; HR: 0.99; 95% CI: 0.59-1.65 (**Fig. 1C**). Based on the strong correlation in LUAD, we evaluated protein expression in a panel of LUAD tumors and normal tissues using an antibody that detects COX6B2 (**Fig. 1D**; Supplementary Fig. S1B-D). We found that COX6B2 expression is low or undetectable in normal lung, but present in all tumor-derived tissues irrespective of stage and grade (**Fig. 1D**; Supplementary Fig. S1E). This expression in tumors does not have an apparent correlation with either the presence or absence of COX6B1, the somatic isoform of COX6B2 (Supplementary Fig. S1F). A similar pattern is also observed in LUAD-derived cell lines (**Fig. 1E**). Immunofluorescence of endogenous COX6B2 in intact LUAD cells revealed specific localization to the mitochondria as judged by overlap with Tom20, a mitochondrial resident protein (**Fig. 1F**). Thus, COX6B2 is frequently expressed in LUAD, correlates with poor survival and when ectopically expressed can localize to its native mitochondrial location.

COX6B2, but not COX6B1, enhances oxidative phosphorylation in LUAD

To investigate whether COX6B2 supports OXPHOS when ectopically expressed in tumors, we generated a LUAD cell line that overexpresses COX6B2 protein ~3-fold (HCC-515-COX6B2-V5). (**Fig. 2A**). This overexpression is not associated with an increase in mitochondrial DNA or total mitochondria (**Fig. 2B**). We then measured the oxygen consumption rate (OCR) at baseline and following exposure to electron transport chain perturbagens. This analysis revealed a significant enhancement in basal, ATP-linked, maximal and reserve OCR (**Fig. 2C**). A similar trend is observed in an independent LUAD cell line, H2122 expressing COX6B2-V5 (**Fig. 2D** and **E**). The OCR increase is associated with an elevation in total ATP in both cell lines (**Fig. 2F**). In addition, we observe elevated NAD^+/NADH in COX6B2-V5 cells, indicative of an overall increase in electron transport activity (**Fig. 2G**). We did not observe a significant or reproducible alteration in extracellular acidification rate (ECAR) in either setting (**Fig. 2H**). We also studied whether COX6B2's somatic isoform, COX6B1, was sufficient to enhance OCR (**Fig. 2I**). COX6B1-V5 expression appears to decrease OCR for each parameter (**Fig. 2J**), consistent with prior biochemical studies where COX6B1 removal enhances the activity of CcO (15).

COX6B2 enhances cytochrome c oxidase activity and stabilizes mitochondrial supercomplexes

To further characterize the impact of COX6B2, we directly assessed CcO activity in permeabilized cells (19,20). Complex III was inhibited with antimycin A, and exogenous cytochrome c electron donors (TMPD, ascorbate) were then added for direct stimulation of CcO. Compared to control cells, COX6B2-V5 expressing cells exhibited enhanced CcO activity (**Fig. 3A**). This finding suggests that COX6B2 is rate limiting subunit of CcO. Recently, a number of reports have suggested that tissue specific CcO isoforms may promote supercomplex formation that could selectively and specifically increase ATP production

(26,27). To test this possibility for COX6B2, we used BN-PAGE analysis to separate supercomplexes in control and COX6B2-V5 expressing cells. While overall levels of supercomplexes were not changed (based on Coomassie blue staining), immunoblotting revealed increased incorporation of COX6B2 into $I+III_2+IV_n$ and III_2+IV higher order complexes (**Fig. 3B**). Supercomplexes are hypothesized to promote local channeling of substrates, trapping of reactive intermediates and/or subunit stabilization. The enhanced activity is induced without a compensatory increase in ROS (26). Indeed, COX6B2 overexpressing cells do not display a concomitant induction of superoxide (**Fig. 3C**). These data suggest that COX6B2 expression promotes formation of mitochondrial supercomplexes that could enhance ATP production while limiting oxidative stress that can lead to irreversible cellular damage.

COX6B2 enhances cell proliferation and promotes growth advantages in low oxygen

We next investigated whether the expression of COX6B2 was sufficient to enhance the growth of LUAD cells. We observed an increase of ~50% in DNA synthesis as measured by EdU incorporation (**Fig. 4A**). Notably, an increase is not observed for COX6B1, which did not increase OCR (**Fig. 4A**, middle panel, **Fig. 2J**). The increase in DNA synthesis corresponded with an enhanced population double rate (**Fig. 4B**, (-) Pyruvate column). Mitochondrial OXPHOS has been linked to proliferation via regulation of the NAD^+/NADH ratio, which is elevated in COX6B2 overexpressing cells (**Fig. 2G**) (28,29). Consistent with this model, supplementation with pyruvate, an electron acceptor which drives NAD+ production, largely diminishes the proliferative effects of COX6B2 overexpression (**Fig. 4B**). Similar proliferative differences are also observed when cells are grown in the absence of extracellular matrix, suggesting that COX6B2 promotes tumorigenic behaviors (**Fig. 4C**).

Tissue specific expression of CcO subunits can be induced by certain environmental conditions that permit adaptation to changing physiological conditions. In particular, hypoxia is reported to regulate CcO subunit expression and permit continued respiration in low oxygen

(27,30,31). Therefore, we cultured control expressing and COX6B2-V5 cells in 2.5% O_2 for four days, measuring the cell population every 24 hours. Under these conditions, control cells exhibit ~30% decrease in growth rate, while the growth of COX6B2-V5 expressing is unaltered (**Fig. 4D**). Given this phenotype, we examined whether COX6B2 is regulated in response to low oxygen. Indeed, we observed a greater than two fold increase in COX6B2 but not COX6B1 mRNA following 12 hours of 2.5% oxygen (**Fig. 4E**). This accumulation of mRNA was associated with stabilization of COX6B2 protein (**Fig. 4F**). Collectively, these data suggest that the enhanced electron transport activity in COX6B2 expressing cells confers a selective advantage by promoting key tumorigenic behaviors including unrestrained proliferation, anchorage independent growth and enhanced survival in hypoxia.

Depletion of COX6B2 impairs mitochondrial electron transport chain function in LUAD cells.

Given the pro-proliferative phenotype following COX6B2 expression, we next examined the consequences of its depletion on OXPHOS and tumor cell viability. Reduction of COX6B2 protein in either a stable (shRNA) or transient (siRNA) fashion led to a decrease in basal, ATP-linked, maximal and reserve OCR (**Fig. 5A** and **B**). We were unable to establish a stable clone of COX6B2 deleted cells by CRISPR/Cas9. However, COX6B2 directed CRISPR/Cas9 did generate a population with reduced COX6B2 protein expression (Supplementary Fig. S2A). In line with the si and shCOX6B2 data, these cells also exhibit attenuated OCR (Supplementary Fig. S2A and B). The reduction in OCR following COX6B2 depletion is accompanied by a reduction in the NAD^+/NADH ratio. (**Fig. 5C**). In addition, total cellular ATP is decreased following COX6B2 depletion in a panel of COX6B2-expressing LUAD cell lines (**Fig. 5D**). Consistent with a loss of electron transport chain function, depletion of COX6B2 resulted in decreased mitochondrial membrane potential (**Fig. 5E**) and increased reactive oxygen species

(**Fig. 5F**). Collectively, these findings indicate that COX6B2 is essential for respiration and ATP production in tumor cells.

Depletion of COX6B2 decreases cell survival and induces cell apoptosis and senescence

Based on the observed decrease in OCR, we asked whether tumor cell viability was diminished following COX6B2 depletion in LUAD cells. Depletion of COX6B2 for 9 days, results in a decrease in EdU incorporation, a phenotype recapitulated in the sgCOX6B2 cells (**Fig. 6A**; Supplementary Fig. S2C). Furthermore, these cells are severely compromised in their ability to grow in the absence of an extracellular matrix (**Fig. 6B;** Supplementary Fig. S2D). We next examined the underlying mechanism(s) leading to the loss of viability. We measured programmed cell death markers and observed an activation of cleaved caspase-3 and cleaved PARP in COX6B2 depleted cells (**Fig. 6C**; Supplementary Fig. S2E). These changes are accompanied by an increase Annexin-V staining, demonstrating activation of caspase-dependent programmed cell death (**Fig. 6D**). Visual inspection of COX6B2 depleted cultures also revealed a population of cells that are flattened, accumulate vacuoles, and in some cases, are multi-nucleated, feature reminiscent of senescence (**Fig. 6E**). Staining of these cells revealed an increase in β-galactosidase, suggesting induction of a cellular senescence program (**Fig. 6F**). Thus, COX6B2 is essential for survival of LUAD tumor cells as its suppression reduces ATP, compromises mitochondrial integrity and leads to a loss of cell viability, either through apoptosis or senescence.

COX6B2 is necessary and sufficient for tumor growth *in vivo*

We next sought to determine whether COX6B2 was necessary and/or sufficient for tumor growth *in vivo*. Thus, we implanted control and COX6B2-V5 HCC-515 cells into the flank of FOXn1^{nu} (nude) mice. Importantly, tumors engrafted subcutaneously encounter a highly hypoxic environment (~0.08 - 0.8% O_2) (32). In agreement with the cell line data, we

observed enhanced growth of COX6B2-V5 expressing cells in vivo (**Fig. 7A**). After 39 days, COX6B2-V5 tumors exhibit a 4X greater mass than control (**Fig. 7B**). In the converse experiment, we xenografted control and shCOX6B2 cells in the flank of immunocompromised mice. Complementing the gain of function phenotype observed, we found that depletion of COX6B2 severely reduces tumor growth and final tumor mass (**Fig. 7C** and **D**). Taken together, our findings indicate that the anomalous expression of COX6B2 is both necessary and sufficient for growth of LUAD tumors.

Discussion

Our data indicate that COX6B2 enhances CcO activity leading to an increase cellular ATP production. This is the first study of COX6B2 function, which has remained obscure in both tumor cells and sperm since its discovery (10). The function of COX6B2 appears to differ from COX6B1, which did not positively induce OXPHOS when overexpressed, a finding consistent with previous biochemical analyses that indicate removal of COX6B1 enhances CcO activity (15). Genetic studies demonstrate that human mutations in COX6B1 reduce assembly of CcO and other ETC complexes. Based on this cumulative data, we hypothesize that COX6B1 (and perhaps B2) are essential for assembly and regulation of CcO. In normal tissues, COX6B1 negatively regulates CcO to prevent the generation of excessive and unused energy and also damaging ROS. In sperm, where ATP demand is high, COX6B2 expression promotes mitochondrial supercomplex formation, permitting enhanced ATP output and limiting ROS production that would otherwise damage DNA (33). This function may be particularly important during early tumorigenesis, where a highly hypoxic environment can lead to proliferative arrest and excessive ROS generation. We propose that tumor cells that express and engage the COX6B2-based, sperm-specific mechanism can overcome this innate barrier to transformation that would otherwise restrict cell survival.

One of the most surprising aspects of our study was the loss of tumor cell viability following the depletion of COX6B2. As COX6B2 enhances ATP production, its loss would be expected to reduce ATP and slow proliferation, but not kill the cells. Tumor cell glycolytic pathways should also theoretically compensate for reduced energy generation. Moreover, the presence of COX6B1 should be able to support CcO function. Instead, we observe ROS production and an exit from the cell cycle either to death or senescence. This finding implies that these cells are highly dependent upon OXPHOS for survival. In addition, the loss of COX6B2 may promote apoptosis due to a collapse of mitochondrial membrane potential and cytochrome c egress (34,35).

The majority of tumor metabolism studies have focused on the contribution of the Warburg effect and have led to the notion that OXPHOS is dispensable for many transformed cells. However, a growing body of evidence indicates that OXPHOS is essential for tumor cell division and survival. First, OXPHOS contributes to >80% of total ATP production in tumor cells, which is essential for satisfying the demands of proliferation and tumor progression (36-38). Second, OXPHOS provides electron acceptors to generate metabolic intermediates (e.g. aspartate) that are required for continued cell division (29). Third, tumor cells exhibit enhanced sensitivity to inhibitors of OXPHOS (39,40). Fourth, isoform switching of CcO subunits is observed in tumors and is associated with aggressive malignant behaviors (41-43). Finally, OXPHOS is upregulated and essential for survival during ER-stress, hypoxia and glucose limiting conditions, and exposure to targeted therapies (27,31,44,45). Based on these and a vast array of additional data, it is accepted that inhibition of OXPHOS is a tractable therapeutic entry point for treating cancer (46). Indeed, extensive studies with metformin have demonstrated anti-proliferative activities and reduction of tumor incidence through the inhibition of Complex I (46). However, this and other ETC inhibitors cannot discriminate between tumor or normal cells, limiting their therapeutic window. We propose that COX6B2 is an acquired trait

that is essential for OXPHOS in LUAD and perhaps additional cancers. At minimum, elevated COX6B2 protein expression is a functional enrollment biomarker for OXPHOS inhibitor based treatment. Moreover, COX6B2 structural elements that are distinct from COX6B1 could represent targets for small molecule inhibitors. Finally, due to expression in an immune privileged site, CTAs have long been considered ideal targets for immunotherapy. However, no objective criterion exists to prioritize them for immunotherapy. We propose that COX6B2 represents an ideal candidate for immunotherapy because it has a bona fide tumorigenic function. Specifically, sequence differences between COX6B2 and COX6B1 could permit antigen recognition by patient immune cells and thus act as targets of adoptive T-cell transfer.

Author Contributions

AWW, C-CC and PM, designed experiments, analyzed data and wrote the paper. C-CC, KM and JW conducted experiments.

Acknowledgements

The authors thank Melanie Cobb and Zane Gibbs for critical review of the manuscript. We acknowledge the assistance of the University of Texas Southwestern Tissue Resource, a shared resource at the Simmons Comprehensive Cancer Center, which is supported in part by the National Cancer Institute under award number 5P30CA142543.

Declaration of Interests

The authors declare no competing interests.

References

1. Hunder NN, Wallen H, Cao J, Hendricks DW, Reilly JZ, Rodmyre R*, et al.* Treatment of metastatic melanoma with autologous CD4+ T cells against NY-ESO-1. N Engl J Med **2008**;358:2698-703

2. Gjerstorff MF, Andersen MH, Ditzel HJ. Oncogenic cancer/testis antigens: prime candidates for immunotherapy. Oncotarget **2015**;6:15772-87
3. Gibbs ZA, Whitehurst AW. Emerging Contributions of Cancer/Testis Antigens to Neoplastic Behaviors. Trends Cancer **2018**;4:701-12
4. Viphakone N, Cumberbatch MG, Livingstone MJ, Heath PR, Dickman MJ, Catto JW*, et al.* Luzp4 defines a new mRNA export pathway in cancer cells. Nucleic Acids Res **2015**;43:2353-66
5. Nichols BA, Oswald NW, McMillan EA, McGlynn K, Yan J, Kim MS*, et al.* HORMAD1 Is a Negative Prognostic Indicator in Lung Adenocarcinoma and Specifies Resistance to Oxidative and Genotoxic Stress. Cancer Res **2018**;78:6196-208
6. Odet F, Duan C, Willis WD, Goulding EH, Kung A, Eddy EM*, et al.* Expression of the gene for mouse lactate dehydrogenase C (Ldhc) is required for male fertility. Biol Reprod **2008**;79:26-34
7. Krisfalusi M, Miki K, Magyar PL, O'Brien DA. Multiple glycolytic enzymes are tightly bound to the fibrous sheath of mouse spermatozoa. Biol Reprod **2006**;75:270-8
8. Li SS, O'Brien DA, Hou EW, Versola J, Rockett DL, Eddy EM. Differential activity and synthesis of lactate dehydrogenase isozymes A (muscle), B (heart), and C (testis) in mouse spermatogenic cells. Biol Reprod **1989**;40:173-80
9. Maxfield KE, Taus PJ, Corcoran K, Wooten J, Macion J, Zhou Y*, et al.* Comprehensive functional characterization of cancer-testis antigens defines obligate participation in multiple hallmarks of cancer. Nat Commun **2015**;6:8840
10. Huttemann M, Jaradat S, Grossman LI. Cytochrome c oxidase of mammals contains a testes-specific isoform of subunit VIb--the counterpart to testes-specific cytochrome c? Mol Reprod Dev **2003**;66:8-16
11. Kadenbach B, Huttemann M. The subunit composition and function of mammalian cytochrome c oxidase. Mitochondrion **2015**;24:64-76
12. Sampson V, Alleyne T. Cytochrome c/cytochrome c oxidase interaction. Direct structural evidence for conformational changes during enzyme turnover. Eur J Biochem **2001**;268:6534-44
13. Tsukihara T, Aoyama H, Yamashita E, Tomizaki T, Yamaguchi H, Shinzawa-Itoh K*, et al.* The whole structure of the 13-subunit oxidized cytochrome c oxidase at 2.8 A. Science **1996**;272:1136-44
14. Abdulhag UN, Soiferman D, Schueler-Furman O, Miller C, Shaag A, Elpeleg O*, et al.* Mitochondrial complex IV deficiency, caused by mutated COX6B1, is associated with encephalomyopathy, hydrocephalus and cardiomyopathy. Eur J Hum Genet **2015**;23:159-64
15. Weishaupt A, Kadenbach B. Selective removal of subunit VIb increases the activity of cytochrome c oxidase. Biochemistry **1992**;31:11477-81
16. Wright WE, Shay JW. Inexpensive low-oxygen incubators. Nat Protoc **2006**;1:2088-90
17. Gyorffy B, Surowiak P, Budczies J, Lanczky A. Online survival analysis software to assess the prognostic value of biomarkers using transcriptomic data in non-small-cell lung cancer. PLoS One **2013**;8:e82241
18. de Almeida MJ, Luchsinger LL, Corrigan DJ, Williams LJ, Snoeck HW. Dye-Independent Methods Reveal Elevated Mitochondrial Mass in Hematopoietic Stem Cells. Cell Stem Cell **2017**;21:725-9 e4
19. Salabei JK, Gibb AA, Hill BG. Comprehensive measurement of respiratory activity in permeabilized cells using extracellular flux analysis. Nat Protoc **2014**;9:421-38
20. Divakaruni AS, Rogers GW, Murphy AN. Measuring Mitochondrial Function in Permeabilized Cells Using the Seahorse XF Analyzer or a Clark-Type Oxygen Electrode. Curr Protoc Toxicol **2014**;60:25 2 1-16
21. Gui DY, Sullivan LB, Luengo A, Hosios AM, Bush LN, Gitego N*, et al.* Environment Dictates Dependence on Mitochondrial Complex I for NAD+ and Aspartate Production and Determines Cancer Cell Sensitivity to Metformin. Cell Metab **2016**;24:716-27

22. Jha P, Wang X, Auwerx J. Analysis of Mitochondrial Respiratory Chain Supercomplexes Using Blue Native Polyacrylamide Gel Electrophoresis (BN-PAGE). Curr Protoc Mouse Biol **2016**;6:1-14
23. Wittig I, Braun HP, Schagger H. Blue native PAGE. Nat Protoc **2006**;1:418-28
24. Ikeda K, Shiba S, Horie-Inoue K, Shimokata K, Inoue S. A stabilizing factor for mitochondrial respiratory supercomplex assembly regulates energy metabolism in muscle. Nat Commun **2013**;4:2147
25. Gallegos ZR, Taus P, Gibbs ZA, McGlynn K, Gomez NC, Davis I*, et al.* EWSR1-FLI1 Activation of the Cancer/Testis Antigen FATE1 Promotes Ewing Sarcoma Survival. Mol Cell Biol **2019**;39
26. Maranzana E, Barbero G, Falasca AI, Lenaz G, Genova ML. Mitochondrial respiratory supercomplex association limits production of reactive oxygen species from complex I. Antioxid Redox Signal **2013**;19:1469-80
27. Ikeda K, Horie-Inoue K, Suzuki T, Hobo R, Nakasato N, Takeda S*, et al.* Mitochondrial supercomplex assembly promotes breast and endometrial tumorigenesis by metabolic alterations and enhanced hypoxia tolerance. Nat Commun **2019**;10:4108
28. Birsoy K, Wang T, Chen WW, Freinkman E, Abu-Remaileh M, Sabatini DM. An Essential Role of the Mitochondrial Electron Transport Chain in Cell Proliferation Is to Enable Aspartate Synthesis. Cell **2015**;162:540-51
29. Sullivan LB, Gui DY, Hosios AM, Bush LN, Freinkman E, Vander Heiden MG. Supporting Aspartate Biosynthesis Is an Essential Function of Respiration in Proliferating Cells. Cell **2015**;162:552-63
30. Hayashi T, Asano Y, Shintani Y, Aoyama H, Kioka H, Tsukamoto O*, et al.* Higd1a is a positive regulator of cytochrome c oxidase. Proc Natl Acad Sci U S A **2015**;112:1553-8
31. Fukuda R, Zhang H, Kim JW, Shimoda L, Dang CV, Semenza GL. HIF-1 regulates cytochrome oxidase subunits to optimize efficiency of respiration in hypoxic cells. Cell **2007**;129:111-22
32. Helmlinger G, Yuan F, Dellian M, Jain RK. Interstitial pH and pO2 gradients in solid tumors in vivo: high-resolution measurements reveal a lack of correlation. Nat Med **1997**;3:177-82
33. Agarwal A, Virk G, Ong C, du Plessis SS. Effect of oxidative stress on male reproduction. World J Mens Health **2014**;32:1-17
34. Smaili SS, Hsu YT, Sanders KM, Russell JT, Youle RJ. Bax translocation to mitochondria subsequent to a rapid loss of mitochondrial membrane potential. Cell Death Differ **2001**;8:909-20
35. Tai H, Wang Z, Gong H, Han X, Zhou J, Wang X*, et al.* Autophagy impairment with lysosomal and mitochondrial dysfunction is an important characteristic of oxidative stress-induced senescence. Autophagy **2017**;13:99-113
36. Rao S, Mondragon L, Pranjic B, Hanada T, Stoll G, Kocher T*, et al.* AIF-regulated oxidative phosphorylation supports lung cancer development. Cell Res **2019**;29:579-91
37. Lissanu Deribe Y, Sun Y, Terranova C, Khan F, Martinez-Ledesma J, Gay J*, et al.* Mutations in the SWI/SNF complex induce a targetable dependence on oxidative phosphorylation in lung cancer. Nat Med **2018**;24:1047-57
38. Zu XL, Guppy M. Cancer metabolism: facts, fantasy, and fiction. Biochem Biophys Res Commun **2004**;313:459-65
39. Nayak AP, Kapur A, Barroilhet L, Patankar MS. Oxidative Phosphorylation: A Target for Novel Therapeutic Strategies Against Ovarian Cancer. Cancers (Basel) **2018**;10
40. Scotland S, Saland E, Skuli N, de Toni F, Boutzen H, Micklow E*, et al.* Mitochondrial energetic and AKT status mediate metabolic effects and apoptosis of metformin in human leukemic cells. Leukemia **2013**;27:2129-38
41. Oliva CR, Markert T, Gillespie GY, Griguer CE. Nuclear-encoded cytochrome c oxidase subunit 4 regulates BMI1 expression and determines proliferative capacity of high-grade gliomas. Oncotarget **2015**;6:4330-44
42. Zhang K, Wang G, Zhang X, Huttemann PP, Qiu Y, Liu J*, et al.* COX7AR is a Stress-inducible Mitochondrial COX Subunit that Promotes Breast Cancer Malignancy. Sci Rep **2016**;6:31742

43. Minton DR, Fu L, Mongan NP, Shevchuk MM, Nanus DM, Gudas LJ. Role of NADH Dehydrogenase (Ubiquinone) 1 Alpha Subcomplex 4-Like 2 in Clear Cell Renal Cell Carcinoma. Clin Cancer Res **2016**;22:2791-801
44. Balsa E, Soustek MS, Thomas A, Cogliati S, Garcia-Poyatos C, Martin-Garcia E*, et al.* ER and Nutrient Stress Promote Assembly of Respiratory Chain Supercomplexes through the PERK-eIF2alpha Axis. Mol Cell **2019**;74:877-90 e6
45. Guieze R, Liu VM, Rosebrock D, Jourdain AA, Hernandez-Sanchez M, Martinez Zurita A*, et al.* Mitochondrial Reprogramming Underlies Resistance to BCL-2 Inhibition in Lymphoid Malignancies. Cancer Cell **2019**;36:369-84 e13
46. Weinberg SE, Chandel NS. Targeting mitochondria metabolism for cancer therapy. Nat Chem Biol **2015**;11:9-15

Figure 1. COX6B2 mRNA expression correlates with poor outcome in LUAD. **A-C.** Kaplan-Meier curves for overall survival (OS) and time to first progression (FP) in NSCLC (A) lung adenocarcinoma (LUAD) (B) and lung squamous (LUSC) patients (C). **D and E.** Whole cell lysates of LUAD tumors and LUAD cell lines were immunoblotted with indicated antibodies. Molecular weight (MW) markers are indicated. **F.** Representative confocal images of endogenous COX6B2 in HCC-515 cells. Tom20 is used as a mitochondrial marker. Images were shown as Z-stack maximum projection from 0.3 μm-thick-images. Scale bar, 10 μm.

Figure 1 Cheng et al

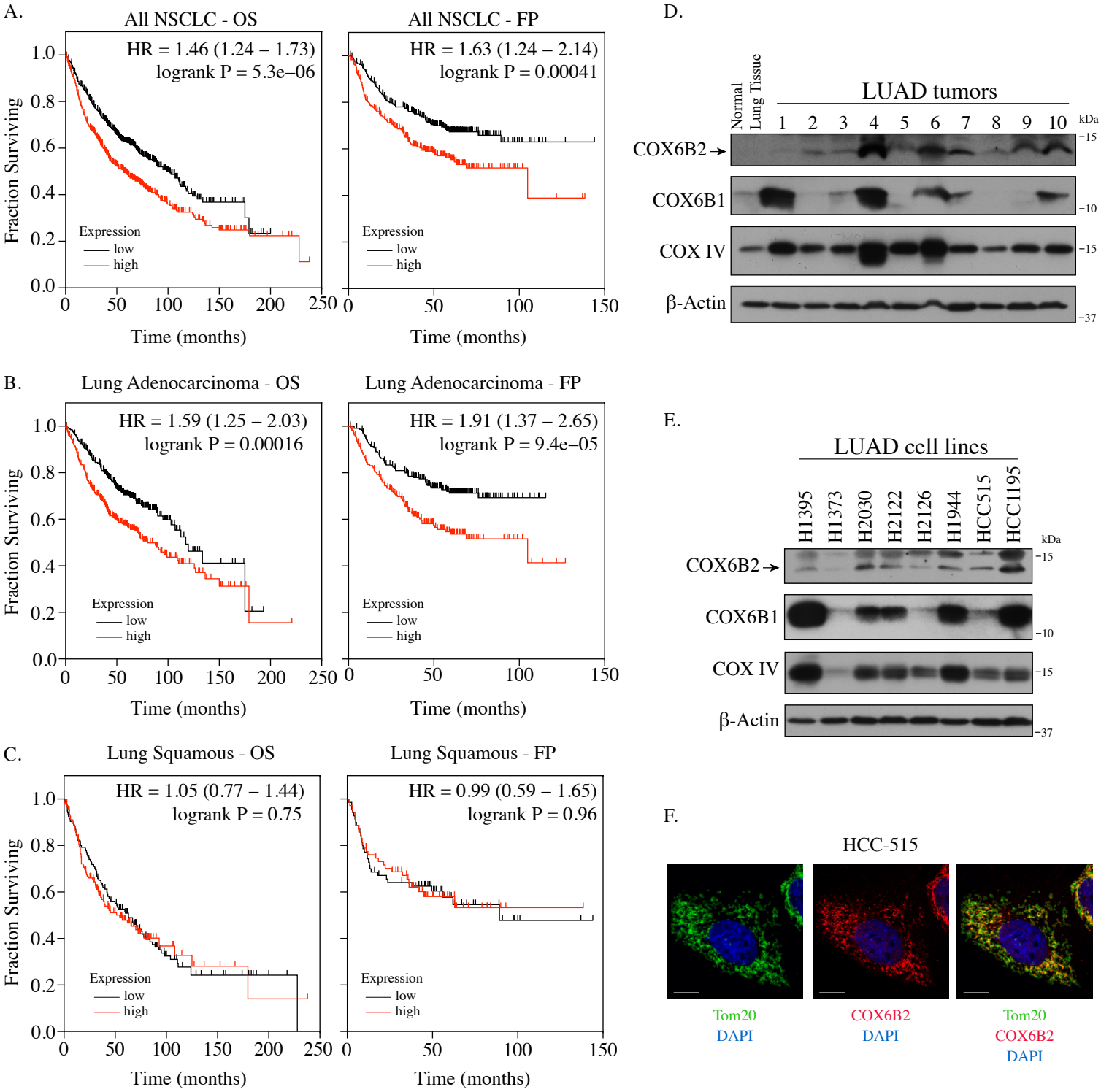

Figure 2. COX6B2 expression enhances mitochondrial respiratory activity. **A.** Left: Whole cell lysates from HCC-515 cells +/- COX6B2-V5 were immunoblotted with indicated antibodies. MW markers are indicated. Right: quantitation of COX6B2 protein expression. Bars represent mean (n = 4) ± SD. **B.** Left: Mitochondrial DNA content. Bars represent mean (n = 2) ± range). Right: Quantification of total mitochondria by Mitotracker green in indicated cell lines. Bars represent mean (n = 3) ± SD). **C**. Left: Oxygen consumption rate (OCR) as a function of time in indicated cell lines following exposure to electron transport chain complex inhibitors. Right: Mean and distribution of individual values for basal, ATP-linked, maximal and reserve OCRs. *P* values calculated by Student's *t*-test. (n = 6) **D.** Left: Whole cell lysates from H2122 cells +/- COX6B2-V5 were immunoblotted with indicated antibodies. MW markers are indicated. Right: quantitation of COX6B2 protein expression. Bars represent mean (n = 3) ± SD. **E.** As in C (n = 8). **F.** ATP content of indicated cell lines. Bars represent mean ± SEM (n ≥ 6). HCC-515 *P* value calculated by Student's *t*-test and H2122 *P* value calculated by Mann-Whitney test. **G.** NAD^+/NADH measurement in indicated cell lines. Bars represent mean ± SEM (n ≥ 5). *P* value calculated by Student's *t*-test. **H.** Basal extracellular acidification rate (ECAR) are presented as mean ± SEM (n ≥ 6) from CTRL and COX6B2-V5 cells of HCC-515 and H2122 cells. *P* value calculated by Student's *t*-test. **I.** Immunoblots of indicated whole cell lysates with specified antibodies. MW markers are indicated. **J.** As in C. Bars represent mean ± SEM (n ≥ 6). Basal and ATP-link OCR *P* value calculated by Student's *t*-test. Maximal OCR and reserve capacity *P* value calculated by Mann-Whitney test.

Figure 2 Cheng et al

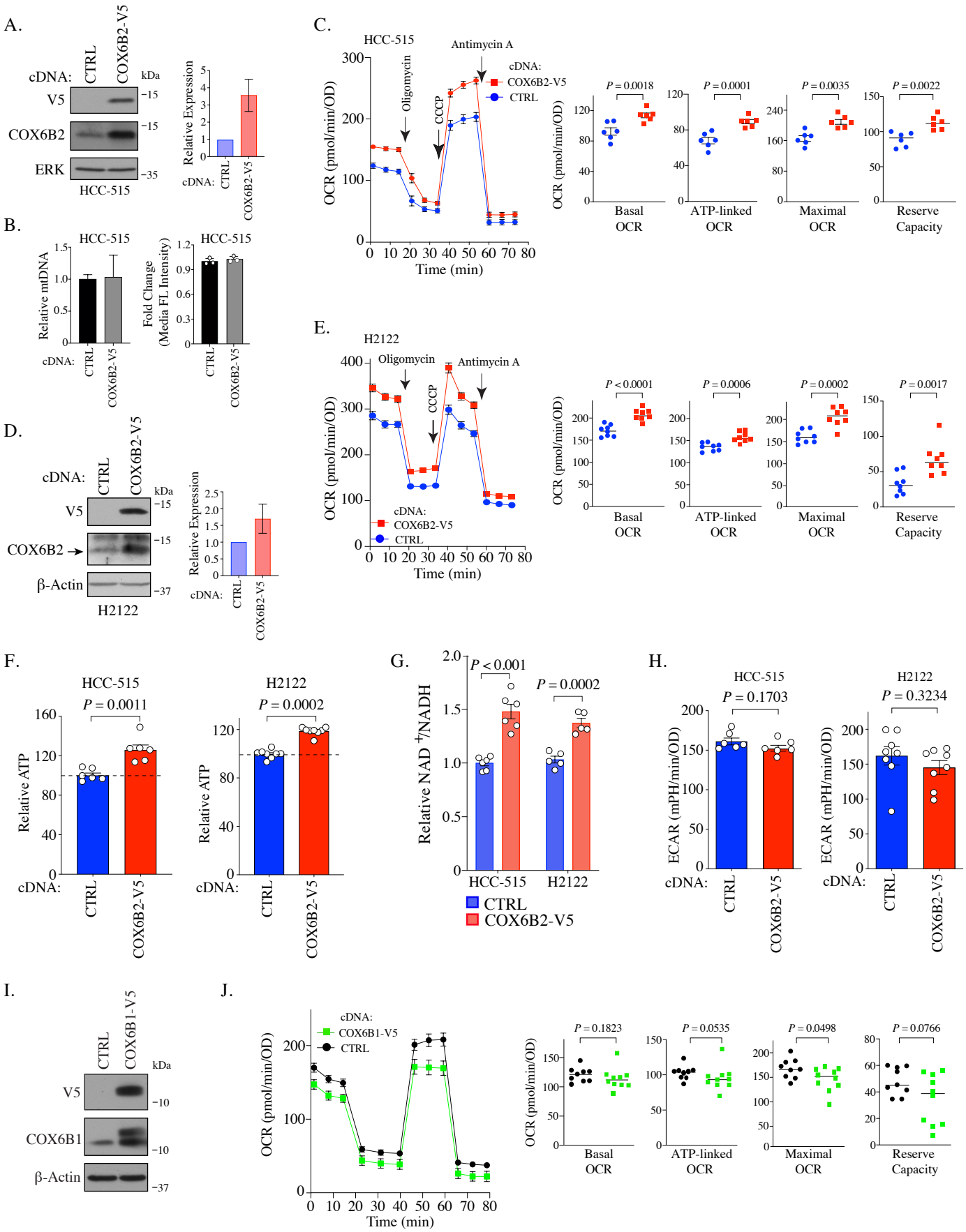

Figure 3. COX6B2 enhances cytochrome c oxidase activity of OXPHOS without increasing ROS production. **A.** Left: Schematic of treatment to measure CcO activity. antA, Antimycin A; Cyt c, Cytochrome C; ATP Syn, ATP synthase. Right: CcO activity, measured by oxygen consumption rate in the presence of TMPD/ascorbate. Bars represent mean ± SEM (n ≥ 8). *P* value calculated by Student's *t*-test. **B.** Left: Indicated lysates were run on a BN-PAGE gel and stained with Colloidal Blue or (Right:) immunoblotted with anti-COX6B2. Representative image of n=2. MW markers are indicated. **C.** Relative mitochondrial ROS (superoxide) in indicated cell lines. Bars represent mean (n = 5) ± SEM. *P* value calculated by Student's *t*-test.

Figure 3 Cheng et al

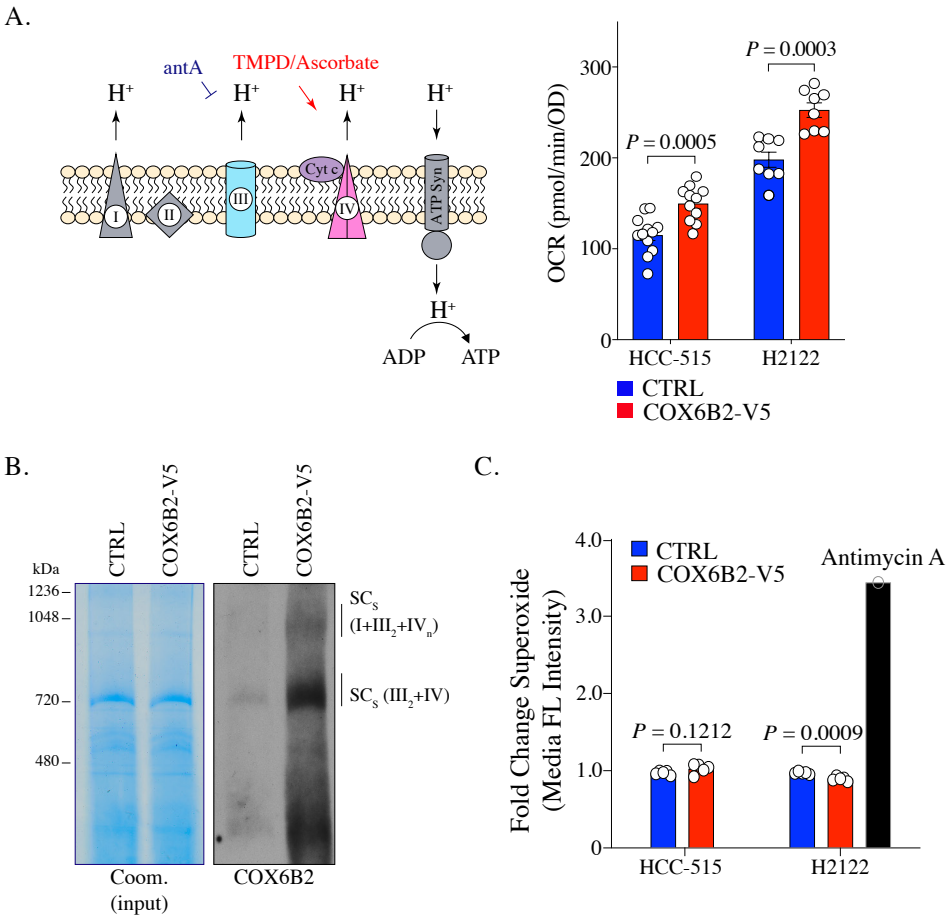

Figure 4. COX6B2 promotes cell division. **A.** Percentage of cells positive for EdU incorporation in indicated samples. Values represent the mean ± SEM (n ≥ 9). *P* value calculated by Student's *t*-test. **B.** Population doubling rate in indicated samples in the absence or presence of 1mM pyruvate. Bars represent means ± SEM (n = 6). *P* value calculated by Student's *t*-test. **C.** Representative images of soft agar assays for indicated cell lines. Graphs represent mean colony numbers in indicated cell lines (n = 6). Arrows indicate formed colonies. *P* value calculated by Student's *t*-test. **D.** Relative HCC-515 cell number at indicated times in hypoxia. Bars represent mean ± SEM (n = 8). *P* value calculated by Student's *t*-test. **E.** Average mRNA expression of COX6B2 measured following 12 hours of hypoxia culture in HCC-515 cells. Bars represent mean (n = 6) ± SEM. *P* calculated by Student's *t*-test. **F.** Whole cell lysates from indicated cell lines were immunoblotted with indicated antibodies. Hypoxia exposure was for 12 hours. Representative immunoblots from n = 3. MW markers are indicated.

Figure 4 Cheng et al

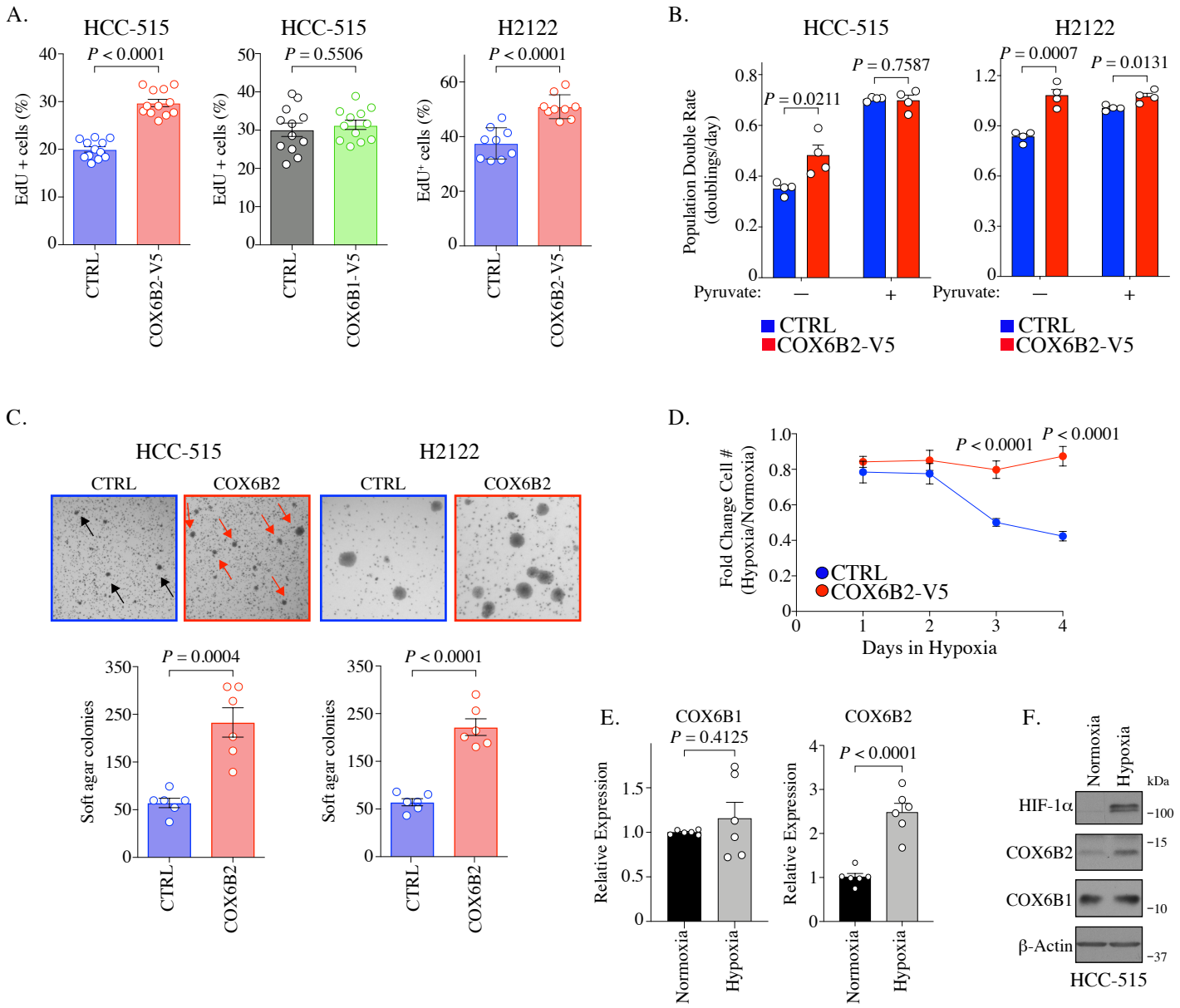

Figure 5. Depletion of COX6B2 impairs mitochondrial function. **A** and **B.** Left: Oxygen consumption rate (OCR) as a function of time in indicated cell lines following exposure to electron transport chain complex inhibitors. n≥4 ± SEM. Right: Bars represent mean ± SEM 20 minutes following the addition of each drug (on left). n≥4. *P* values calculated by Student's *t*-test. **C.** Relative NAD^+/NADH measurement in indicated cell lines. Bars represent mean ± SEM (n = 4). *P* value calculated by Student's *t*-test. **D.** Relative ATP content in indicated cell lines transfected with indicated siRNAs for 96 hours. Bars represent mean ± SEM (n = 6), **** $P < 0.0001$; *** $P < 0.005$ calculated by Student's *t*-test. **E.** Left panels: Flow cytometry measurement of following JC-1 labelling of indicated HCC-515 cells. Right graph: Bars represent mean of the aggregate to monomer ratio (red/green) in indicated cell lines ± SEM (n = 3). *P* value calculated by Student's *t*-test. **F.** Indicated cell lines were labelled with CM-H2DCFDA to measure H_2O_2 as described in material and methods. Bars represent mean fold change in median fluorescent intensities ± SEM (n = 4). *P* value calculated by Student's *t*-test.

Figure 5 Cheng et al

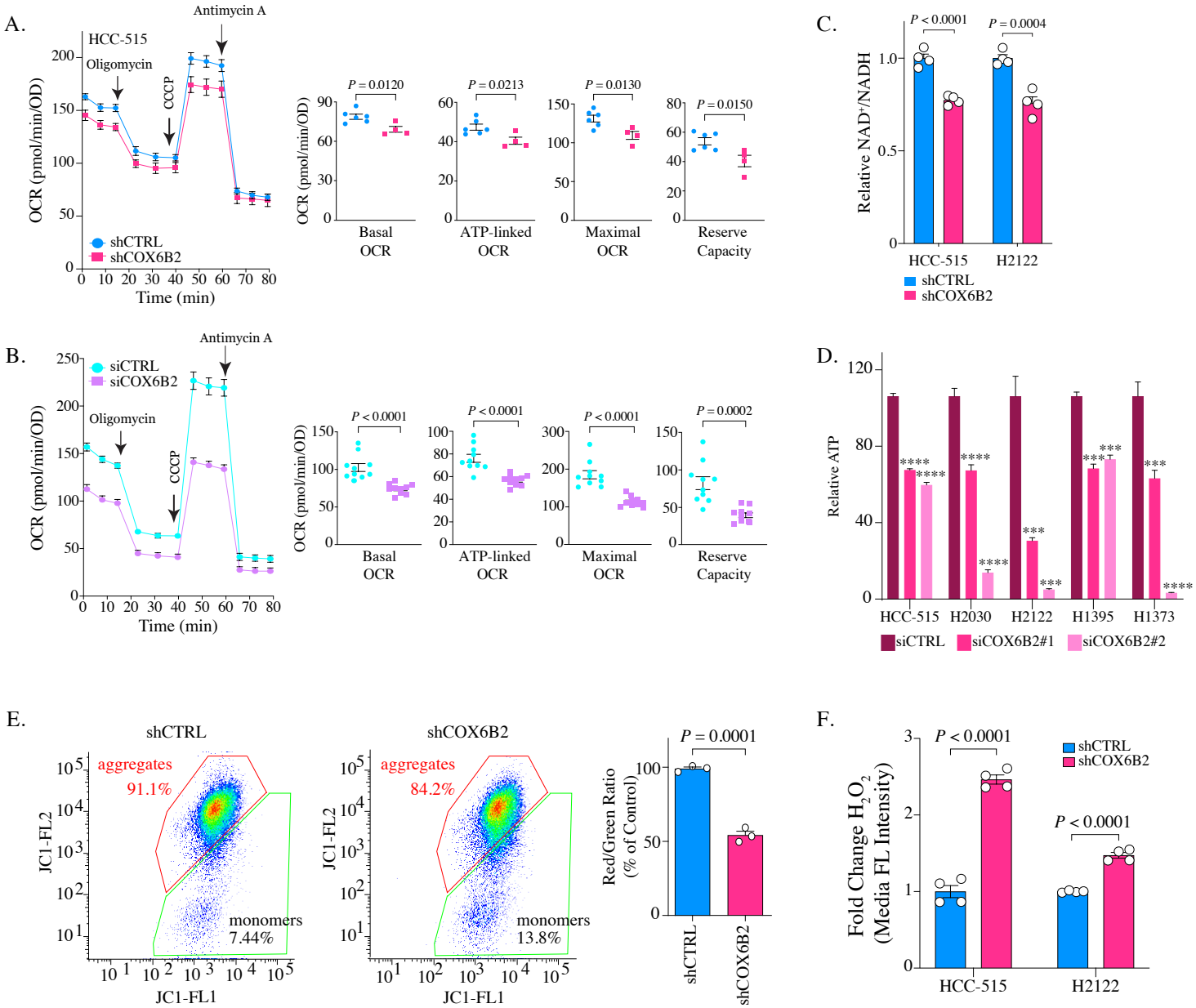

Figure 6. COX6B2 is essential for tumor cell viability and survival. **A.** Left: Representative images of EdU staining in indicated cells. (EdU, green; Hoechst, blue). Scale bar, 100 μm. Right: Quantitation of EdU-positive cells. Bars represent the mean ± SEM (n ≥ 12). *P* value calculated by Student's *t*-test. **B.** Left: Representative images of colonies in soft agar. Arrows indicate formed colonies. Right: Bars represent relative mean colony numbers ± SEM (n = 6). *P* value calculated by Student's *t*-test. **C.** Representative immunoblots of whole cell lysates of indicated cells blotted with indicated antibodies. MW markers are indicated. **D.** Left: Representative scatter plots of Annexin V staining in indicated cells. Bars represent mean fold change ± SEM (n = 6). *P* calculated by Student's *t*-test. **E.** Representative phase contrast images of indicated cells. Arrowheads indicate the flattened senescence morphology with vacuole accumulation and multinucleation. Scale bar, 100 μm. **F.** Representative images of senescence-associated-β-galactosidase staining in indicated cells. Scale bar, 100 μm. Bars represent mean ± SEM (n ≥ 8). *P* calculated by Student's *t*-test.

Figure 6 Cheng et al

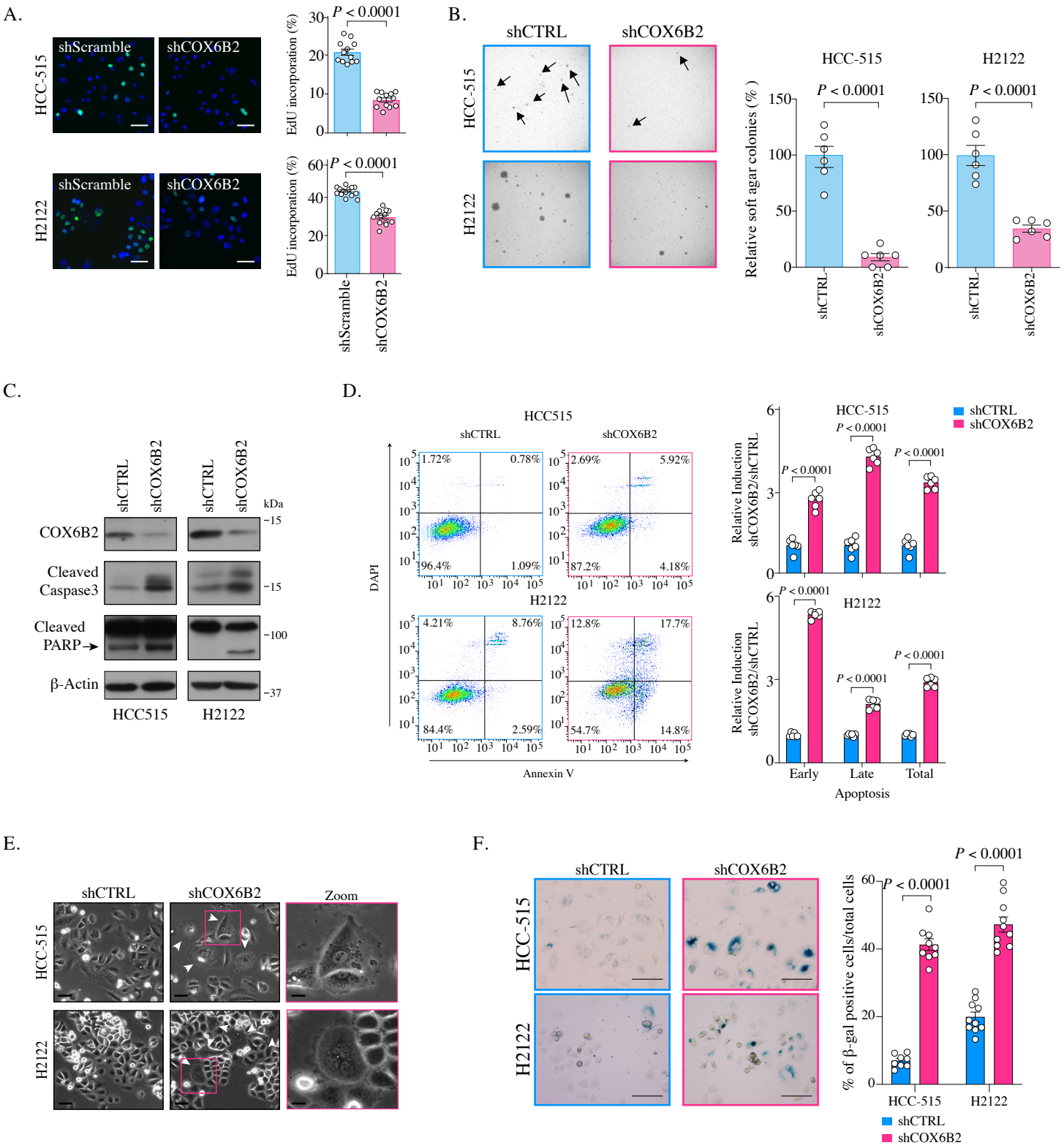

Figure 7.

COX6B2 supports tumor growth *in vivo*. **A** and **C.** Xenograft experiments in indicated cell lines. Tumor volumes were measured using calipers on indicated days. Each data point represents mean ± SEM (n = 5). *P* value calculated by Student's *t*-test. **B** and **D.** Left: images of individual tumors (ruler indicates cm). Right: mass of excised tumors from indicated cell lines. Bars represent mean ± SEM (n = 5). *P* value calculated by Student's *t*-test.

Figure 7 Cheng et al

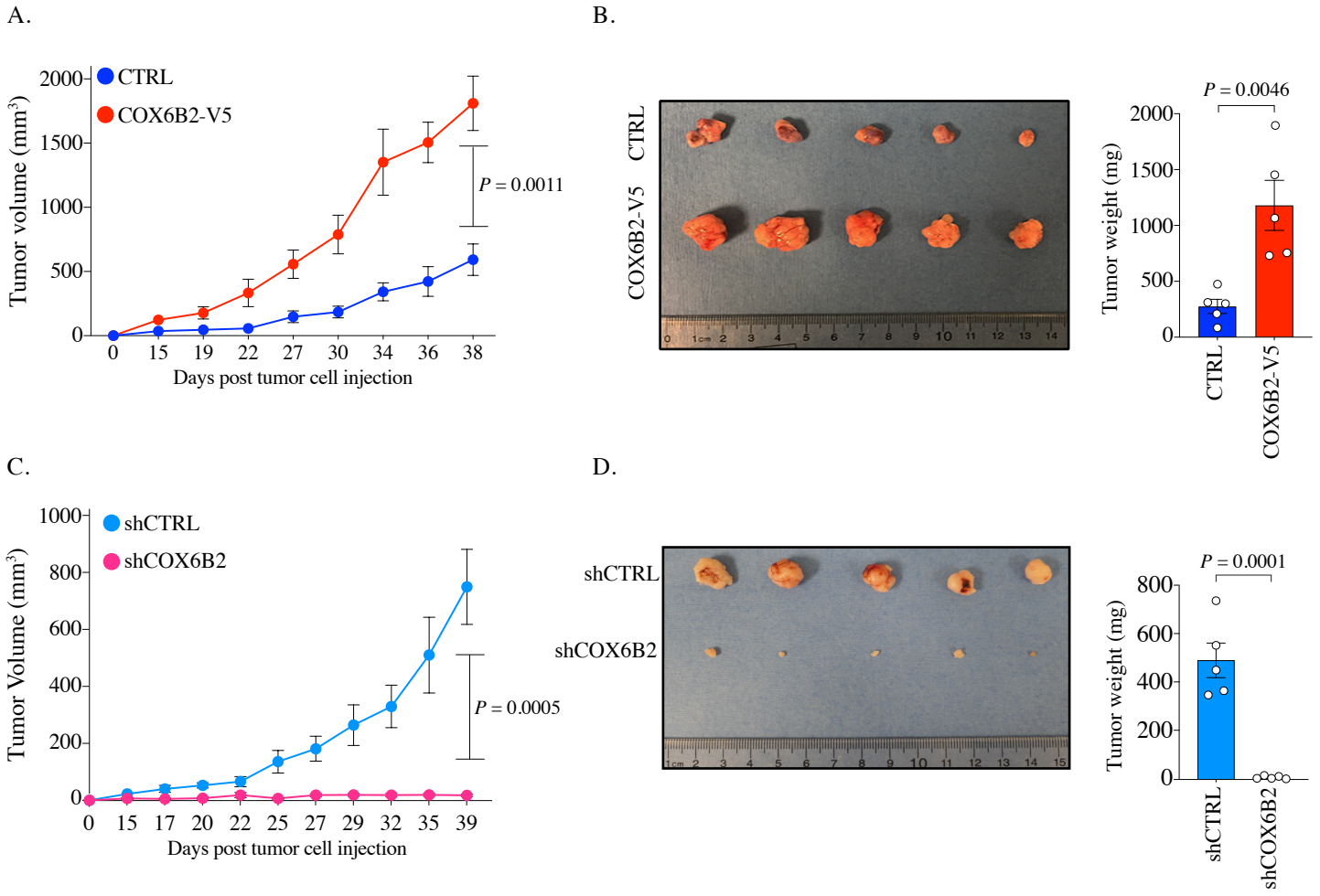

Supplementary Figure 1. COX6B2 expression in LUAD**. A**. Z-score of caspase3/7 activity screening in indicated cell lines. **B**-**D**. Whole cell lysates from indicated cell lines were immunoblotted with indicated antibodies. **E**. Clinical data associated with tumors used in Fig. 1D. **F**. Pearson's correlation analysis of COX6B1 and COX6B2 protein expression in LUAD tumors and cell lines.

Supplementary Figure 1 Cheng et al

A.

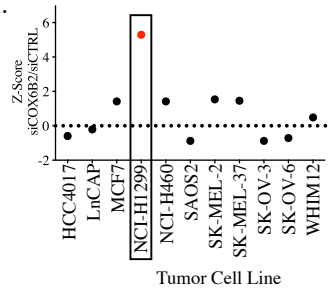

B.

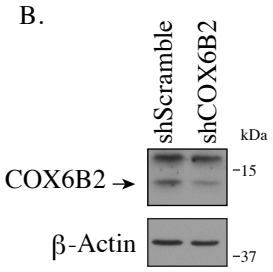

C.

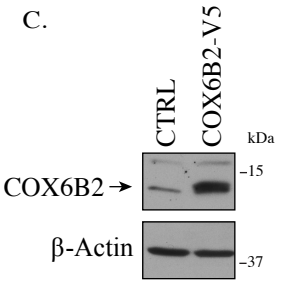

D.

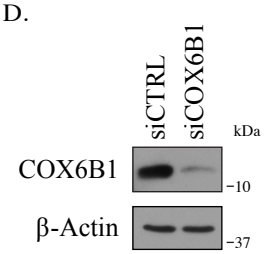

E.

No	Pathology	Stage
1	Adenocarcinoma: 40% acinar, 30% papillary, 20% lepidic, 10% micropapillary	IB
2	Adenocarcinoma 90% solid with 10% acinar subtype	IIB
3	Solid adenocarcinoma with mucin (AB-PAS only) Nearly 100% solid	IIA
4	Adenocarcinoma, solid 60%, acinar 40%	IIIB
5	Adenocarcinoma, papillary-predominant (papillary - 85%; micropapillary - 15%)	IIB
6	Adenocarcinoma, acinar/cribriform (60%), solid (40%)	IIIA
7	Adenocarcinoma, acinar predominant	IB
8	Adenocarcinoma	IIB
9	Adenocarcinoma, solid subtype	IIA
10	Adenocarcinoma	IIB

F.

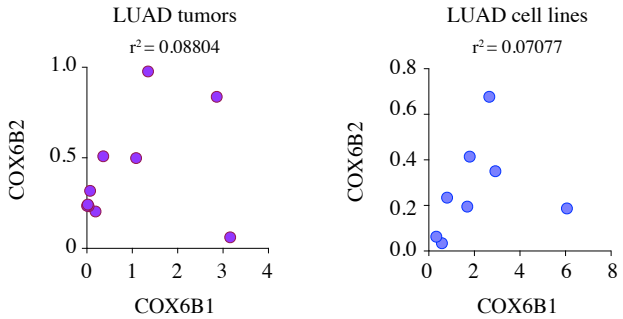

Supplementary Figure 2. Phenotypes following COX6B2 depletion by sgRNA**. A**. Representative images of western blots from whole cell lysates of indicated cells. **B**. OCR was measured as a function of tumor for each parameter in indicated cells. Bars represent mean ± SD (n = 7). *P* value calculated by Student's *t*-test. **C**. (Left) Proliferation rates and (Right) the percentage of EdU-positive cells of indicated cells. Bars represent mean ± SEM (n ≥ 5). *P* value calculated by Student *t* test. **P* < 0.05, ****P* < 0.001, *****P* < 0.0001. **D**. Representative images of colonies in soft agar. Arrows indicate formed colonies. Graphs represent relative colony numbers in indicated cells. Bars represent mean ± SEM (n = 6). *P* value calculated by Student's *t*-test. **E**. Representative images and quantitative data of western blots from whole cell lysates of indicated cells and immunoblotted with indicated antibodies. Bars represent mean (n = 3) ± SD.
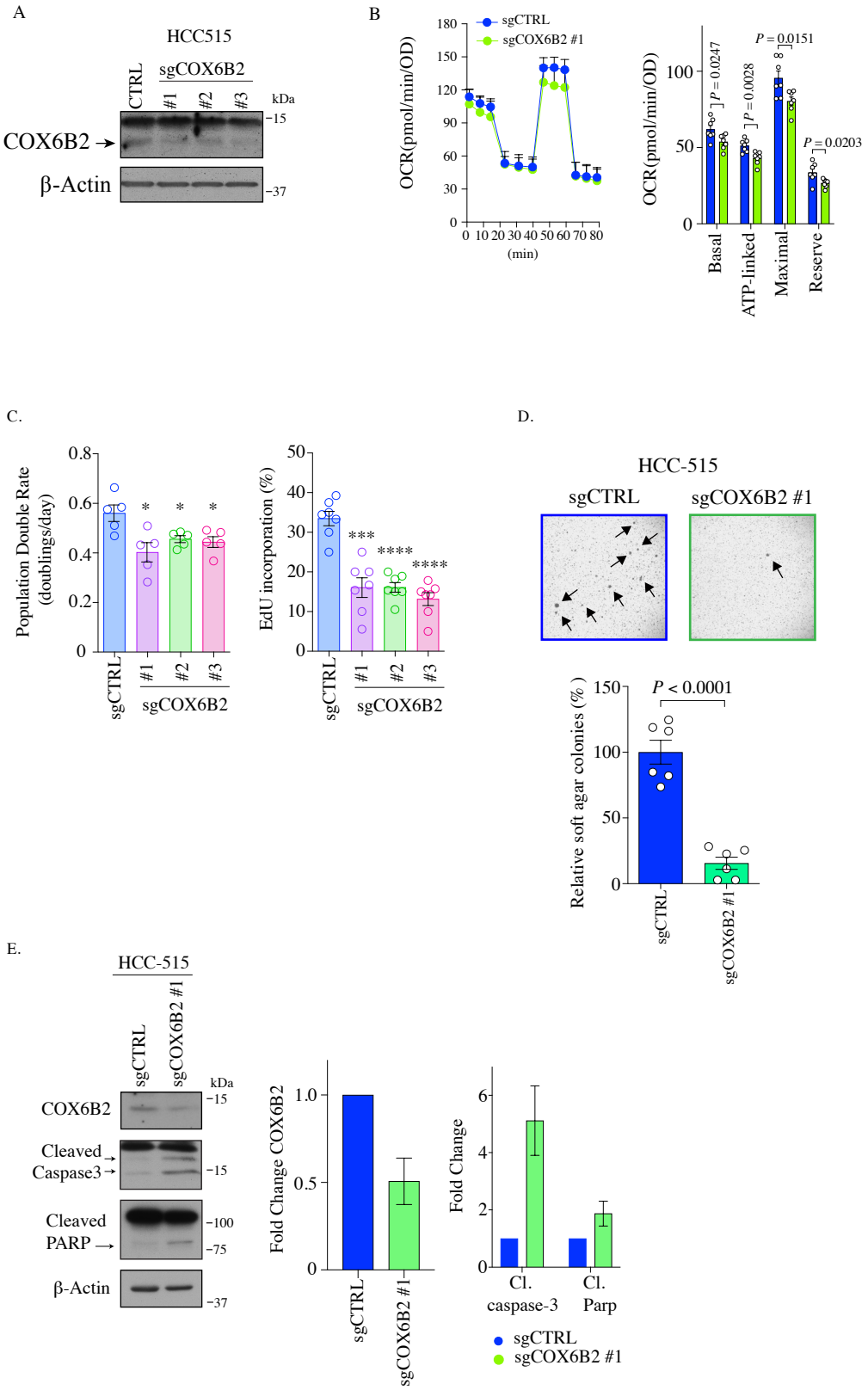
Supplementary Figure 2 Cheng et al